Cdc48 regulates intranuclear quality control sequestration of the Hsh155 splicing factor

Veena Mathew[1], Arun Kumar[1,2], Yangyang K. Jiang[1] , Kyra West[1], Annie S. Tam[1, 2], Peter C. Stirling[1, 2, 3]

[1]Terry Fox Laboratory, British Columbia Cancer Agency, Vancouver, Canada
[2]Department of Medical Genetics, University of British Columbia, Vancouver, Canada
[3]Correspondence to: pstirling@bccrc.ca

Abstract

Cdc48/VCP is a highly conserved ATPase chaperone that plays an essential role in the assembly or disassembly of protein-DNA complexes and in degradation of misfolded proteins. We find that Cdc48 accumulates during cellular stress at intranuclear protein quality control (INQ) sites. Cdc48 function is required to suppress INQ formation under non-stress conditions and to promote recovery following genotoxic stress. Cdc48 physically associates with the INQ substrate and splicing factor Hsh155 and regulates its assembly with partner proteins. Accordingly, *cdc48* mutants have defects in splicing and show spontaneous distribution of Hsh155 to INQ aggregates where it is stabilized. Overall, this study shows that Cdc48 regulates deposition of proteins at INQ and suggests a previously unknown role for Cdc48 in the regulation or stability of splicing subcomplexes.

Keywords: Protein quality control, Cdc48, INQ, Hsh155, splicing, yeast

Introduction

Protein quality control (PQC) refers to the process of triage for non-native, unassembled or mis-localized proteins through a combination of sequestration, degradation and refolding (1). PQC is a part of normal cellular homeostasis and is particularly important during stress when non-native proteins assemble in visible aggregate structures at different subcellular locations. Various proteotoxic stresses elicit such a coordinated PQC response, with the best characterized being heat stress (2), or expression of amyloid-forming proteins (3). PQC responses depend on networks of molecular chaperones, on the action of stress activated protein aggregase and disaggregase activities (1), and on protein degradation by the ubiquitin-proteasome system and autophagy (3, 4).

During stress in yeast, specific types of aggregate structures with different components and behaviors form (5). In the cytoplasm, aggregates at the vacuolar membrane called the Insoluble Protein Deposit (IPOD) are repositories for irreversibly aggregated proteins destined for degradation, such as amyloids(3). Smaller dynamic cytoplasmic aggregates called Q-bodies (quality control bodies) have also been described for protein aggregate reporters such as Ubc9-ts and VHL (6-8). Finally, at the nuclear envelope the juxtanuclear quality control site (JUNQ) forms peripheral to but outside the nucleus, while the intranuclear quality control site (INQ) forms peripheral to and inside the nucleus (3, 9). Most yeast studies of PQC focus on aggregation prone reporter proteins, such as poly-glutamine fragments, temperature-sensitive (ts) mutants or misfolding human proteins (3, 6, 7, 9). Recently, endogenous proteins have been used as markers of aggregate formation, in particular following genotoxic stress (10-12). Following DNA damage, specific nuclear proteins are actively sequestered in INQ structures (10, 11). Focusing on different INQ substrates, it has been suggested that INQ sequestration helps to regulate the replication fork checkpoint (i.e. Mrc1(10)), the activation of DNA repair proteins (i.e. Mus81 (12)), or rewiring of the spliced transcriptome (i.e. Hsh155 (11)).

INQ formation is driven by the small heat shock protein Hsp42, and the aggregase protein Btn2 (13), while INQ dissolution is regulated by Hsp104 and the Hsp70 system (9, 11, 12). Here we show that Cdc48 is also a stress-inducible component on INQ structures and that it plays an enzymatic role in INQ turnover. Cdc48 plays numerous normal and stress responsive roles in cells, including in nuclear PQC (14-17). Here we show that Cdc48 is concentrated at INQ following DNA damage, and that its activity is important to suppress spontaneous aggregation of splicing factor Hsh155 in INQ. Cdc48 physically interacts with Hsh155 even under non-stress conditions and promotes its assembly with partners in the SF3B complex of the spliceosome. Together these results demonstrate a previously unrecognized role for Cdc48 in protein triage to the INQ and suggest unappreciated roles for Cdc48 in splicing.

Results and Discussion

Cdc48-GFP localizes to intranuclear quality control sites

We previously screened hundreds of genome stability regulatory proteins for relocalization in response to DNA damage, and identified uncharacterized stress-induced relocalization of Cdc48-GFP (11). Cdc48 is widely distributed in unstressed cells, but is enriched at a nuclear periphery/ER-localization due to its role in ER-associated degradation (ERAD) (**Figure 1A**). Following methyl methanesulfonate (MMS) treatment, Cdc48 relocalized to nuclear and non-nuclear foci (**Figure 1A**). To test if these foci were INQ, we expressed Cdc48-GFP together with

Hos2-mCherry, a known marker of the INQ (10, 18). Cdc48 foci colocalized with Hos2-mCherry foci, suggesting that Cdc48 was accumulating at INQ following MMS treatment (**Figure 1B**). Cdc48 also colocalized with Hos2 at peripheral aggregates, which may be cytoplasmic PQC (CytoQ) sites (**Figure 1B and C**). We next ablated INQ formation by deleting the chaperones *HSP42* and *BTN2*, which are essential for INQ protein localization (9-11). Cdc48-GFP foci were strongly diminished in MMS-treated *hsp42*Δ or *btn2*Δ cells, showing that INQ formation was essential for Cdc48 foci (**Figure 1D**). Together these experiments suggest that Cdc48 foci mark INQ structures induced by MMS treatment.

Cdc48 ATPase regulates the aggregation and INQ localization of Hsh155

Since Cdc48 functions in protein biogenesis and turnover, we suspected that it might have a functional role at INQ. We assembled a set of *CDC48* ts-alleles, which grew robustly at the permissive temperature of 25°C but exhibited a range of fitness defects (**Fig. S1A**) (19). Examining the localization of an INQ substrate in the most severe allele, *cdc48-4601* (hereafter called *cdc48-4*) (**Fig. S1C**), revealed spontaneous Hsh155-GFP and Hos2-GFP foci at nuclear and cytoplasmic aggregate sites (**Figure 2A** and **Fig. S1B**). MMS treatment further increased the proportion of cells with visible aggregates beyond WT cells (**Figure 2B**). We confirmed that other *CDC48* ts-alleles also increased spontaneous INQ formation to varying degrees (**Figure 2C**). Consistent with a functionally important role, *cdc48-4* alleles were significantly impaired in recovery from a two-hour treatment of MMS (**Figure 2D**). While there are many possible mechanisms for the MMS sensitivity of a *cdc48-ts* allele, our data show that Cdc48 function is important for regulating the INQ localization of Hsh155 in normal and DNA damaging conditions. Finally, since Cdc48 uses its ATPase activity to disassemble or unfold proteins, we tested the ability of enzymatically active or dead alleles to rescue the *cdc48-4* phenotype. While WT *CDC48* plasmids suppressed Hsh155 foci, an ATPase-deficient $cdc48^{E315Q}$ allele could not (**Figure 2E** and **F**)(16). Thus, the Cdc48 ATPase activity is essential to suppress aggregation of Hsh155-GFP into INQ structures.

Cdc48 regulates the stability of Hsh155 and assembly with its partners

If Cdc48 is important for the prevention or dissolution of INQ structures, then it could regulate the stability of INQ substrate proteins under stress. Consistent with this idea, Hsh155-GFP protein was more abundant in the *cdc48-4* mutant, and more stable in cycloheximide chase experiments, than it was in WT (**Figure 3A**). Since cycloheximide treatment can itself affect protein sequestration (7), we also monitored the impact of Cdc48 on Hsh155 lifetime with an orthogonal approach using *in vivo* tandem fluorescent timer (tFT) fusions (20). The ratio of GFP to mCherry fluorescence in Hsh155-tFT fusions is significantly red-shifted in *cdc48-4* cells indicating a longer relative protein lifetime (**Figure 3B and S2A**). These data are consistent with the INQ serving a protective role for substrate proteins as Hsh155 becomes both more abundant and aggregates in *cdc48-4* cells. Cdc48 could affect the stability of Hsh155 through direct protein-protein interactions. Indeed, we observed co-precipitation of Hsh155-GFP with Cdc48-TAP under both untreated and MMS treated conditions (**Figure 3C**).

Hsh155 is a splicing factor that exists in a complex called SF3B with Hsh49 and Cus1. We previously found that Hsh155 disassembled from the SF3B complex upon MMS treatment (11). To assess the potential impact of Cdc48 on SF3B complex stability, we monitored pulldown of Hsh155-GFP in WT or *cdc48-4* cells with or without MMS treatment by co-immunoprecipitation.

Loss of *CDC48* function greatly diminished the presence of the Hsh155-Cus1 complex, even in untreated cells (**Figure 3D**). This suggests that Cdc48 may play a role in the integrity of the SF3B complex even in the absence of DNA damage signals. While *cdc48-4* grew too poorly to easily monitor splicing activity, the *cdc48-3* allele that showed an intermediate induction of Hsh155 foci (**Figure 2C**) did show reduced splicing flux in a LacZ-based splicing efficiency assay (**Figure 3E**) (21, 22).

Context and perspective

Spatial control of PQC is a fundamental feature of stress responses in eukaryotic cells (23). Here we show that Cdc48, a key regulator of numerous cellular PQC activities, is also associated with INQ where it interacts, reduces the accumulation, or speeds the turnover, of the INQ substrate Hsh155 (**Figure 3F**). This defines a novel and complementary function for Cdc48 in nuclear protein quality control. Previous studies link Cdc48 and its co-factors to proteostasis of nuclear proteins via the San1 E3 ligase, and the inner nuclear membrane proteins Asi1-Asi3, however we see no significant effect of *SAN1* deletion on INQ (**Fig. S2B**)(16, 17). In addition, Cdc48 regulates protein-DNA complexes, such as the removal of RNA polymerase from damaged DNA(15), the removal of replisomes during DNA replication termination(14), at protein-DNA crosslinks (24), and in the release of condensin complexes (25). Thus, Cdc48 is well-positioned to regulate protein sequestration pathways such as INQ following DNA damage detection. The interaction of Cdc48 with INQ may suggest places to start understanding INQ regulation. Other groups have noted the importance of SUMO to INQ formation (10), and we also find that reducing SUMOylation with *ubc9-ts* (SUMO E2) or *SIZ1* (SUMO E3) deletion reduces INQ localization of Hsh155-GFP in MMS-treated WT or *cdc48-4* cells (**Fig. S2C and D**). Indeed, mutation of the SUMO interacting motif of *CDC48* impairs its ability to rescue *cdc48-4* cells (**Fig. S2E**) (26). However, Hsh155-GFP is not detectably SUMOylated after DNA damage (**Fig. S2F)**. Thus, we believe that more work needs to be done to understand the potential roles of SUMO and Cdc48 coordination in INQ regulation, including the identification of any modified INQ proteins.

Our data specifically implicate Cdc48 in regulating the sequestration, complex formation and stability of the spliceosomal protein Hsh155 within the SF3B complex. We previously found that Hsh155 sequestration may regulate ribosomal protein gene expression through reduced splicing efficiency of ribosomal protein gene transcripts (11). In this regard, it is notable that Cdc48 is also a critical regulator of ribosomal quality control mechanisms and can sense ribosomal stress (27, 28). It is possible that these responses are coordinated during the DNA damage response. Regardless, our data define a new function for Cdc48 in regulating the deposition of proteins at the INQ and potentially in the regulation of splicing complexes. There is currently little evidence linking Cdc48 to splicing. Interestingly, a study of motor neuron transcriptome dynamics during iPS differentiation models of human VCP/Cdc48 mutations in amyotrophic lateral sclerosis showed that abnormal intron retention events were increased in the *Cdc48/VCP*-mutated cells (29). Thus, a role for Cdc48 in splicing across species is possible, and we hope that additional research will elucidate if and how Cdc48 may affect splicing.

Figure Legends

Figure 1. *Cdc48 localizes to PQC in a chaperone dependent manner.* (A) Cdc48-GFP fusions relocalize into foci upon MMS treatment (white arrowhead). A schematic on left summarizes the movements in both conditions. (B) Cdc48-GFP foci overlap (white arrowheads in merge) with Hos2-mCherry (mChe) foci after MMS treatment. (C) Quantification of MMS induced Cdc48 in perinuclear (INQ) and peripheral (CytoQ) foci. Mean ± SEM, n= 3 with >100 cells each. (Asterisks show *p*-value (***) p<0.001, Fisher test). (D) Reduction of Cdc48-GFP foci in cells lacking *HSP42* or *BTN2*. Representative images (above) and quantification of percentage of cells with foci (below). *** indicates p<0.001. Error bars are mean± SEM, n= 3 with >50 cells each. Fisher test. Asterisks show *p*-value thresholds in comparison to WT under the same condition. Scale bar, 5μm and for all subsequent figures.

Figure 2. *Cdc48 ATPase regulates the aggregation and INQ localization of Hsh155*. (A) Visualization of Hsh155-GFP foci in cells with temperature sensitive (ts) alleles of *CDC48* with or without MMS stress at 34°C. White arrowheads show foci in untreated cells. (B) Quantification of foci accumulation in untreated and MMS treated *cdc48-4* strains compared to wild type (WT) strains with or without MMS. (C) Spontaneous Hsh155-GFP foci in three different *CDC48* mutant alleles at 34°C. (D) Growth curve analysis of *cdc48-4* after 2hrs of MMS treatment and washout compared to WT strains ± MMS washout at 34°C. The dotted line represents the range wherein all data points significantly differ from WT after MMS washout. N=3 with triplicates in each. Error bars represent mean± SEM, two way ANOVA with Tukey's posthoc test, p-value ranges from <0.05- <0.0001. Significant differences between untreated and treated cells are indicated in the interval, *p<0.05. (E and F) Rescue of Hsh155-GFP foci formation by *CDC48-wt* but not $CDC48^{E315Q}$ ATPase-deficient allele. E is a representative image of data quantified in F. For B, C and F quantifications: Error bars are mean± SEM, n= 3 with >50 cells each. Fisher test, Asterisks show *p*-value thresholds (*** p<0.001; ** p<0.01; * p<0.05 and non-significant (ns)).

Figure 3. *Direct effects of Cdc48 on Hsh155 stability and function.* (A) Hsh155 protein levels ± CHX by anti-GFP western blotting relative to Pgk1 levels in WT and *cdc48-4* over time. CHX = cycloheximide, UNT = untreated. Shown is the representative blot from three independent experiments. (B) Tandem fluorescent timer (tFT) analysis of Hsh155-mCherry-GFP dual fusion lifetime in the indicated strains with or without MMS treatment. Ratios of GFP (fast maturing) and mCherry (slow maturing) fluorescence in the nucleus are shown. Quantification of fluorescent timer indicates the presence older proteins in the nucleus of *cdc48-4* compared to WT in both conditions. Mean± SEM, three replicates, n ≥ 30 per replicate, Mann-Whitney test, asterisks show *p*-value threshold **** p<0.0001. (C) Physical interaction of Hsh155-GFP and Cdc48-TAP with or without MMS treatment by co-immunoprecipitation and western blotting. Control (GFP only) lanes are mock IPs from cells expressing Hsh155-GFP only. (D) Co-precipitation of Hsh155 with its partner Cus1 in the SF3B complex in *cdc48-4* is disrupted in both untreated and MMS conditions similar to MMS induced WT cells. (E) LacZ splicing reporter assay results in WT or *cdc48-3* treated with MMS. A schematic of the assay (above) shows the intronic versus intronless LacZ constructs that enable quantification of splicing efficiency. Quantification of relative LacZ splicing in untreated and MMS treated normalized to 'no intron' control in both WT and *cdc48-3* cells (below). Mean± SEM, Student t-test, Asterisks

show *p*-value (**) p<0.01. N=5 with individual transformants in triplicates each. (F) Model of Cdc48 as a chaperone for Hsh155 involved in its quality control and sequestration at INQ sites (see main text). Cdc48 binds Hsh155 under normal conditions but its disruption or DNA damage leads to SF3B disassembly. Cdc48 may also play a role in INQ resolution or turnover, explaining why its loss increases INQ.

Supplementary Information

Figure S1. Characterization of the *cdc48-4* allele. (A) Spot dilution assay showing growth sensitivity of different *cdc48-ts* mutant alleles tested at the indicated temperatures. Equal ODs of the indicated strains were serially diluted and spotted on YPD at 25°C, 30°C, 34°C and 37°C. (B) Spontaneous Hos2-GFP foci formation in the *cdc48-4* mutant strain. (C) Schematic of Cdc48 protein domains (N- N-terminal, D1, D2 and Ct- C-terminal) with indicated *cdc48-4* coding mutations (red lines) mapped along the sequence.

Figure S2. Testing potential roles of *SAN1* and SUMO in Cdc48 induced Hsh155-GFP foci formation. (A) Tandem fluorescent timer ratio scoring of nuclear versus peripheral foci fluorescence in the indicated strains with or without MMS. Quantification of fluorescent timer indicates aggregation of older proteins in both INQ and CytoQ of *cdc48-4* compared to WT in both conditions. Mean± SEM, three replicates, n ≥ 30 per replicate, Mann-Whitney test, asterisks show *p*-value threshold **** p<0.0001; non-significant (ns). (B) Hsh155-GFP foci induction in WT or *san1*Δ strains treated with MMS. (C) Hsh155-GFP foci induction by MMS in SUMO regulator mutant strains *ubc9-ts* and *siz1*Δ. (D) Induction of spontaneous Hsh155-GFP foci in *cdc48-4* is reduced by deletion of SUMO E3 ligase *SIZ1*. (E) Spontaneous Hsh155-GFP foci in *cdc48-4* complemented by WT or *cdc48-SIM* mutant bearing plasmids. For B-E quantifications: Error bars are mean± SEM, n= 3 with >50 cells each. Fisher test, Asterisks show *p*-value thresholds (**** p<0.0001; *** p<0.001 and non-significant (ns)). (F) SMT3-hisx7 pulldown assays in untreated or MMS treated cells. DNA damage induced SUMOylation of RFA1 in MMS (30) is shown as a positive control after Ni-NTA bead pulldown (Ni PD). No bands are detectable when blotting for Hsh155-GFP.

Table S1. Yeast strains, primers, plasmids used in this study

Materials and Methods

Yeast strains, MMS treatments, and growth analyses

Yeast strains used in this study including database IDs and genotypes, primers and plasmids are listed in **Table S1**. All strains were in the s288c background and were grown under nutrient rich YPD media or synthetic media lacking amino acids (SC) unless otherwise indicated. Serial dilution assays and growth curve analyses were performed as described (11, 31). Briefly, cells with identical optical density (OD) were serially diluted ten-fold and spotted on the YPD plates with a 48-pin replica pinning manifold and incubated at indicated temperatures for 72 hours. Growth curves were analyzed in a Tecan M200 plate reader monitoring OD600nm every 30 minutes for 48 hours at 30 °C. For all MMS treatment conditions cells were exposed to 0.05%

MMS (~99% Sigma) in synthetic complete media for 2 hours unless otherwise noted. For growth curves, MMS was then washed out and replaced with fresh media.

Live cell imaging, image acquisition, analysis and statistical methods
Imaging and subsequent analysis were performed as described (11). Log-phase yeast were mounted on slides pretreated with concanavalin A, in SC growth media. Immobilized cells were imaged using an Objecktive HCX PL APO 1.40 NA oil immersion 100× objective on an inverted Leica DMi8 microscope with a motorized DIC turret (for Differential Interference Contrast imaging) and a filter cube set for FITC/TRITC (for GFP and m-Cherry fluorescence imaging). The images were captured at room temperature using a scientific complementary metal oxide semiconductor (sCMOS) camera (ORCA Flash 4.0 V2; Hamamatsu) and collected using MetaMorph Premier acquisition software and post processed (including gamma adjustments, counting of cells with/without foci, foci intensity measurements for tandem fluorescent timer (tFT) experiments using ImageJ (National Institutes of Health). For all microscopy experiments, the significance of the differences was determined using Prism5 or higher (Graphpad). For foci intensity measurements in tFT experiments, samples were compared with t-tests or ANOVA; Graphpad performs F-tests for variance as part of this analysis. For comparisons of proportions, Fisher tests were used and p-values were Holm-Bonferroni corrected in the event of multiple comparisons. Sample sizes and specific statistical details for each image analysis are listed in the figure legends.

Co-Immunoprecipitation and western blotting
Co-Immunoprecipitation was performed using yeast strains containing TAP tagged Cus1, Cdc48 and/or GFP tagged Hsh155 treated with or without MMS. TAP tagged proteins was captured using IgG sepharose fast flow beads (Sigma) and proceeded as described (32). Immunoblotting was carried out with mouse anti-GFP (ThermoFisher) and rabbit anti-TAP (ThermoFisher).
For western blots, whole cell extracts were prepared by tricholoroacetic acid (TCA) extraction and blotted with mouse anti-GFP (ThermoFisher), rabbit anti-RFA (Agrisera) or mouse anti-PGK1 (Santa Cruz) antibodies as described (10).

Protein stability time course
Overnight cultures of the indicated strains were diluted below OD 0.2 and allowed to progress into logarithmic phase before collection. The cells were treated with or without cycloheximide (CHX) at a concentration of 200 μg/ml for the indicated time (0-120 minutes). The final concentration of $2x10^7$ cells was collected by centrifugation and the whole cell extracts were prepared by TCA extraction followed by immunoblotting.

Splicing efficiency assay
Splicing assay protocol was adapted and performed as described (21). All measurements were taken with three individual transformants per replicate, totaling five replicates. Cells were struck as a patch on SC-leucine, then replica plated to glycerol-lactate–containing SC medium without leucine (GGL-leu). Cells from each patch were inoculated in liquid GGL-leu media for 2 h at 34°C and induced with final 2% galactose for 1.5 h before treatment with final 0.05% MMS for 30 min. Cells were lysed and assayed for β-galactosidase assay using a Gal-Screen β-galactosidase reporter gene assay system for yeast or mammalian cells (Applied Biosystems) as

per the manufacturer's instructions and read with SpectraMax i3 (Molecular Devices). Relative light units were normalized to cell concentration as estimated by measuring OD600.

Ni-NTA pulldown of SUMOylated proteins
SUMO conjugated proteins were detected by performing protein pulldowns under denaturing conditions as described (33). In brief, strains of interest were transformed with a plasmid containing His-tagged SUMO (Smt3-Hisx7) (Addgene) under the control of a copper inducible promoter. Logarithmically growing cells were harvested at OD_{600nm} 0.6-0.8 to a final concentration of 10^9 cells by centrifugation (4000rpm, 5min at 4°C). Pelleted cells were washed and resuspended in 5ml of pre-chilled water. Cells were then lysed with 800µl of 1.85M NaOH/7.5% (v/v) 2-mercaptoethanol followed by 20 min incubation on ice. Protein precipitation was carried out by adding 800µl 55% TCA on ice for 20 minutes. Precipitates were collected by centrifugation (8000g, 20min, 4°C) and were resuspended in 1ml Buffer A (6M guanidine hydrochloride, 100mM sodium phosphate, 10mM Tris-HCl, pH 8.0) and incubated on a rotating block at room temperature for 1 hour to solubilise the precipitate completely. The resulting solution was then centrifuged (16,000g, 10min, 4°C) and supernatant was transferred to tubes containing 30µl precleared Ni-NTA agarose beads (Qiagen) in the presence of 0.05% Tween-20 and 15mM imidazole. These were incubated overnight on a rotating block at room temperature. Following the binding, the beads were washed twice with Buffer A containing 0.05% Tween-20 and four times with Buffer C (8M Urea, 100mM sodium phosphate, 10mM Tris-HCl, pH 6.3) containing 0.05% Tween-20. Beads were centrifuged (200g, 15s) and supernatant was completely removed. His-SUMO conjugates on the beads were eluted out by adding 30µl HU sample buffer and heating at 70°C for 10min. Resultant protein extracts were subjected to standard western blotting and probed for SUMO and other proteins of interest using antibodies as described above.

Acknowledgements
P.C.S. is funded by a Natural Sciences and Engineering Research Council of Canada (NSERC) Discovery grant and Discovery Accelerator Supplement (RPGIN 2020-04360), and a Canadian Institutes of Health Research (CIHR) Project grant (MOP136982). P.C.S. is a CIHR New Investigator and Michael Smith Foundation for Health Research Scholar.

Author Contributions
VM and PCS designed the project. VM, AK, YKJ, KW, AST collected the data and analyzed the data. VM, AK and PCS wrote the paper.

References

1. Hartl FU, Bracher A, & Hayer-Hartl M (2011) Molecular chaperones in protein folding and proteostasis. *Nature* 475(7356):324-332.
2. Wallace EW, *et al.* (2015) Reversible, Specific, Active Aggregates of Endogenous Proteins Assemble upon Heat Stress. *Cell* 162(6):1286-1298.
3. Kaganovich D, Kopito R, & Frydman J (2008) Misfolded proteins partition between two distinct quality control compartments. *Nature* 454(7208):1088-1095.

4. Kumar R, Nawroth PP, & Tyedmers J (2016) Prion Aggregates Are Recruited to the Insoluble Protein Deposit (IPOD) via Myosin 2-Based Vesicular Transport. *PLoS Genet* 12(9):e1006324.
5. Saarikangas J & Barral Y (2016) Protein aggregation as a mechanism of adaptive cellular responses. *Current genetics* 62(4):711-724.
6. Escusa-Toret S, Vonk WI, & Frydman J (2013) Spatial sequestration of misfolded proteins by a dynamic chaperone pathway enhances cellular fitness during stress. *Nat Cell Biol* 15(10):1231-1243.
7. Zhou C, *et al.* (2014) Organelle-based aggregation and retention of damaged proteins in asymmetrically dividing cells. *Cell* 159(3):530-542.
8. Ruan L, *et al.* (2017) Cytosolic proteostasis through importing of misfolded proteins into mitochondria. *Nature* 543(7645):443-446.
9. Miller SB, *et al.* (2015) Compartment-specific aggregases direct distinct nuclear and cytoplasmic aggregate deposition. *EMBO J* 34(6):778-797.
10. Gallina I, *et al.* (2015) Cmr1/WDR76 defines a nuclear genotoxic stress body linking genome integrity and protein quality control. *Nature communications* 6:6533.
11. Mathew V, *et al.* (2017) Selective aggregation of the splicing factor Hsh155 suppresses splicing upon genotoxic stress. *J Cell Biol*.
12. Saugar I, Jimenez-Martin A, & Tercero JA (2017) Subnuclear Relocalization of Structure-Specific Endonucleases in Response to DNA Damage. *Cell Rep* 20(7):1553-1562.
13. Ho CT, *et al.* (2019) Cellular sequestrases maintain basal Hsp70 capacity ensuring balanced proteostasis. *Nature communications* 10(1):4851.
14. Maric M, Mukherjee P, Tatham MH, Hay R, & Labib K (2017) Ufd1-Npl4 Recruit Cdc48 for Disassembly of Ubiquitylated CMG Helicase at the End of Chromosome Replication. *Cell Rep* 18(13):3033-3042.
15. Verma R, Oania R, Fang R, Smith GT, & Deshaies RJ (2011) Cdc48/p97 mediates UV-dependent turnover of RNA Pol II. *Molecular cell* 41(1):82-92.
16. Gallagher PS, Clowes Candadai SV, & Gardner RG (2014) The requirement for Cdc48/p97 in nuclear protein quality control degradation depends on the substrate and correlates with substrate insolubility. *Journal of cell science* 127(Pt 9):1980-1991.
17. Pantazopoulou M, Boban M, Foisner R, & Ljungdahl PO (2016) Cdc48 and Ubx1 participate in a pathway associated with the inner nuclear membrane that governs Asi1 degradation. *Journal of cell science* 129(20):3770-3780.
18. Tkach JM, *et al.* (2012) Dissecting DNA damage response pathways by analysing protein localization and abundance changes during DNA replication stress. *Nature cell biology* 14(9):966-976.
19. Li Z, *et al.* (2011) Systematic exploration of essential yeast gene function with temperature-sensitive mutants. *Nature biotechnology* 29(4):361-367.
20. Khmelinskii A, *et al.* (2012) Tandem fluorescent protein timers for in vivo analysis of protein dynamics. *Nat Biotechnol* 30(7):708-714.
21. Galy V, *et al.* (2004) Nuclear retention of unspliced mRNAs in yeast is mediated by perinuclear Mlp1. *Cell* 116(1):63-73.
22. Tam AS, *et al.* (2019) Selective defects in gene expression control genome instability in yeast splicing mutants. *Mol Biol Cell* 30(2):191-200.

23. Sontag EM, Vonk WIM, & Frydman J (2014) Sorting out the trash: the spatial nature of eukaryotic protein quality control. *Curr Opin Cell Biol* 26:139-146.
24. Amunugama R*, et al.* (2018) Replication Fork Reversal during DNA Interstrand Crosslink Repair Requires CMG Unloading. *Cell Rep* 23(12):3419-3428.
25. Thattikota Y*, et al.* (2018) Cdc48/VCP Promotes Chromosome Morphogenesis by Releasing Condensin from Self-Entrapment in Chromatin. *Molecular cell* 69(4):664-676 e665.
26. Bergink S*, et al.* (2013) Role of Cdc48/p97 as a SUMO-targeted segregase curbing Rad51-Rad52 interaction. *Nat Cell Biol* 15(5):526-532.
27. Brandman O*, et al.* (2012) A ribosome-bound quality control complex triggers degradation of nascent peptides and signals translation stress. *Cell* 151(5):1042-1054.
28. Defenouillere Q*, et al.* (2013) Cdc48-associated complex bound to 60S particles is required for the clearance of aberrant translation products. *Proceedings of the National Academy of Sciences of the United States of America* 110(13):5046-5051.
29. Luisier R*, et al.* (2018) Intron retention and nuclear loss of SFPQ are molecular hallmarks of ALS. *Nature communications* 9(1):2010.
30. Psakhye I & Jentsch S (2012) Protein group modification and synergy in the SUMO pathway as exemplified in DNA repair. *Cell* 151(4):807-820.
31. Stirling PC*, et al.* (2011) The Complete Spectrum of Yeast Chromosome Instability Genes Identifies Candidate CIN Cancer Genes and Functional Roles for ASTRA Complex Components. *PLoS genetics* 7(4):e1002057.
32. Leung GP, Brown JA, Glover JN, & Kobor MS (2016) Rtt107 BRCT domains act as a targeting module in the DNA damage response. *DNA Repair (Amst)* 37:22-32.
33. Ulrich HD & Davies AA (2009) In vivo detection and characterization of sumoylation targets in Saccharomyces cerevisiae. *Methods in molecular biology* 497:81-103.

Figure1

Mathew et.al

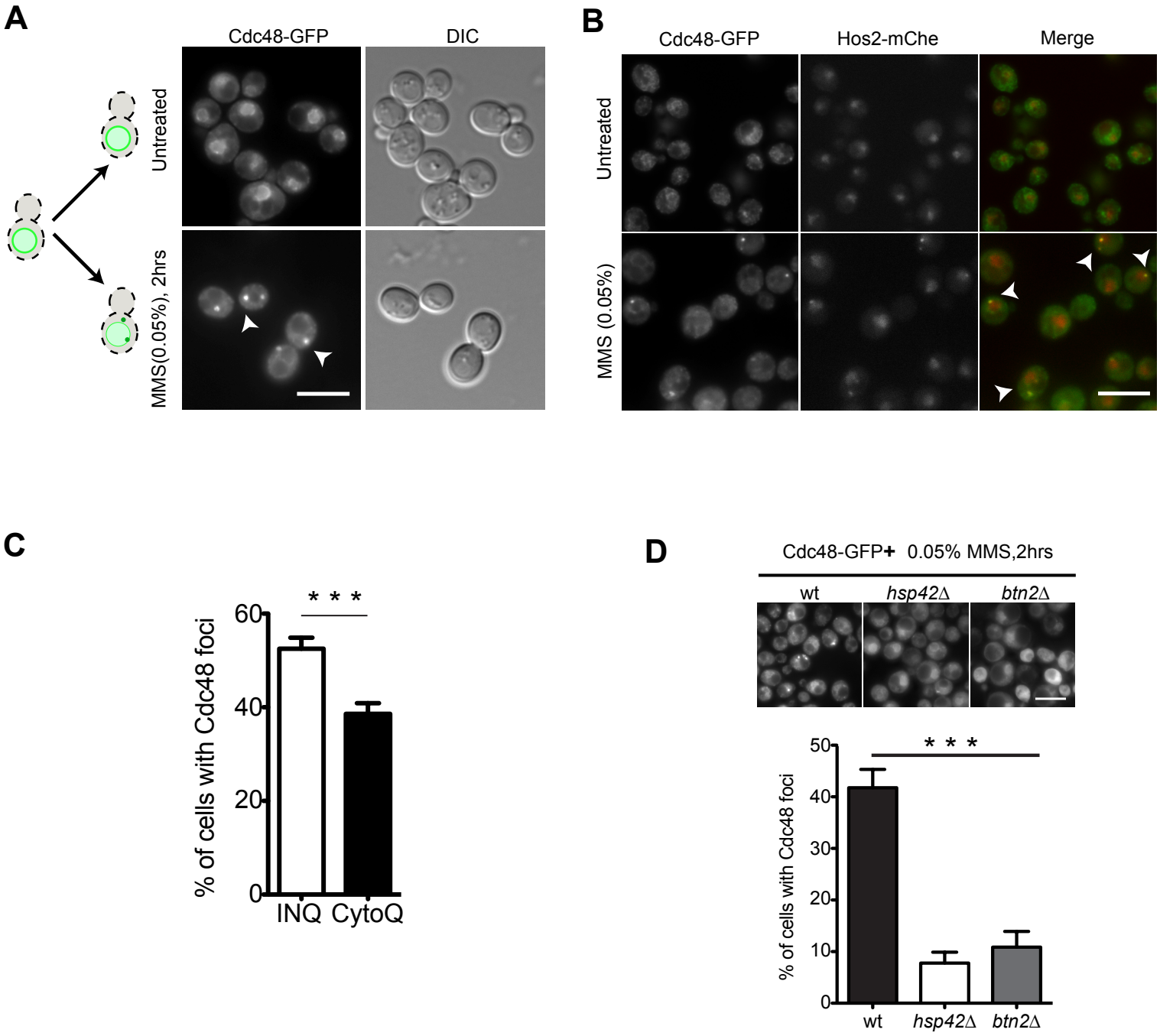

Figure2

Mathew et.al

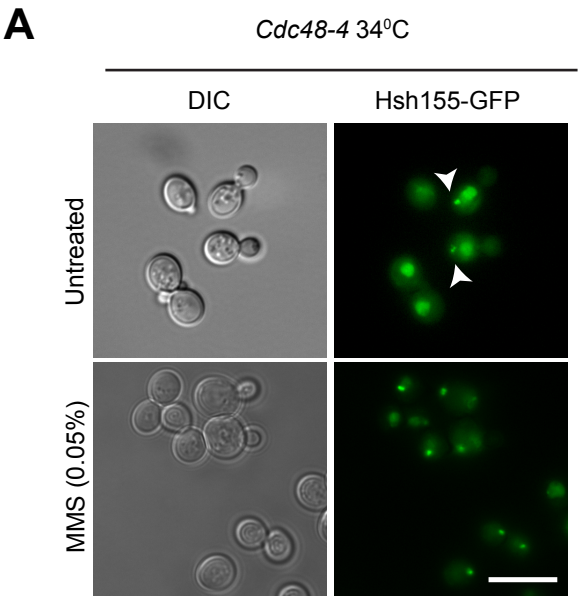

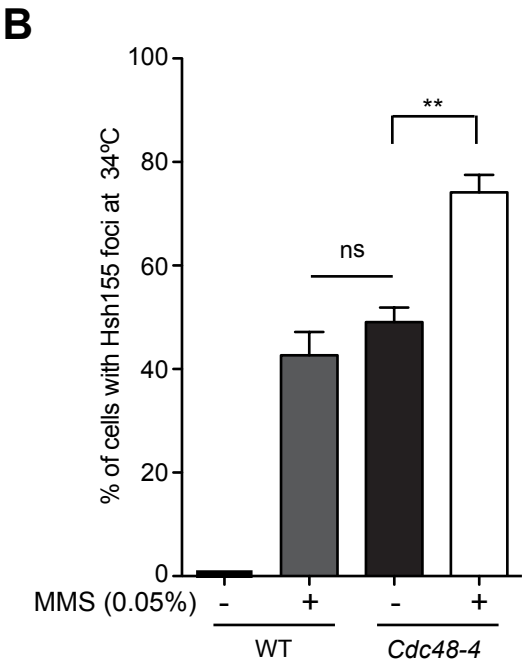

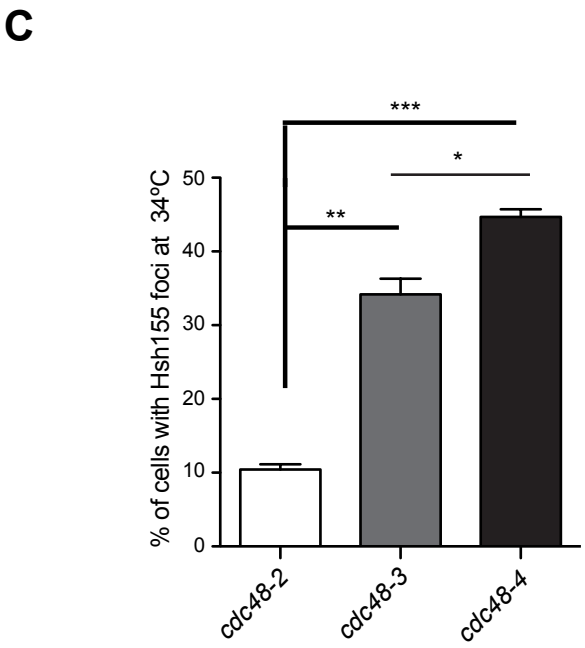

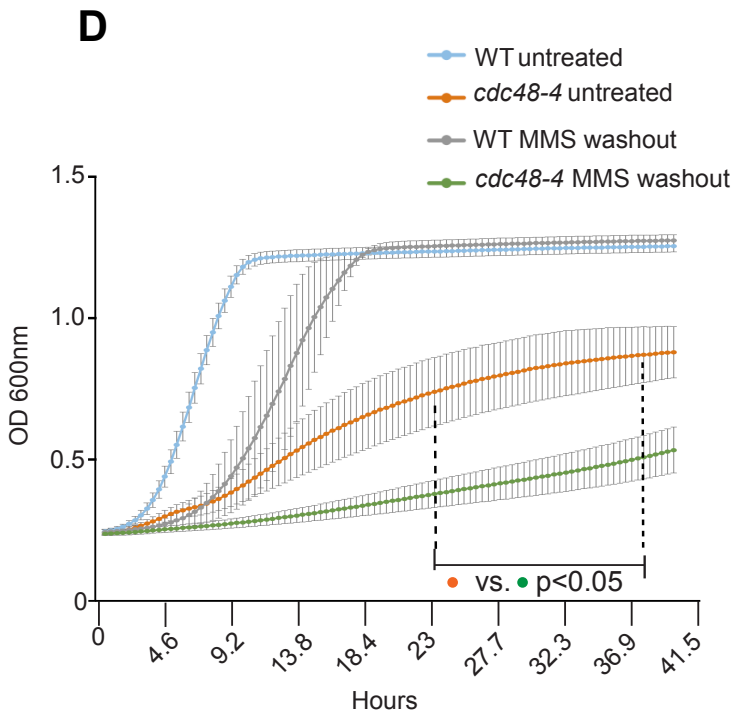

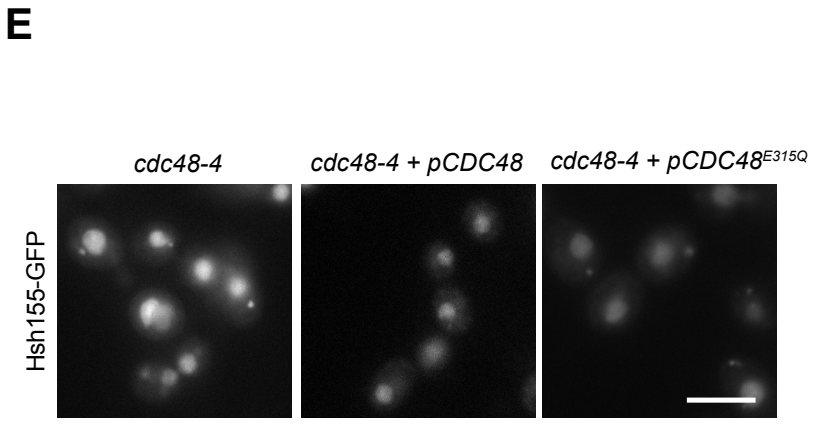

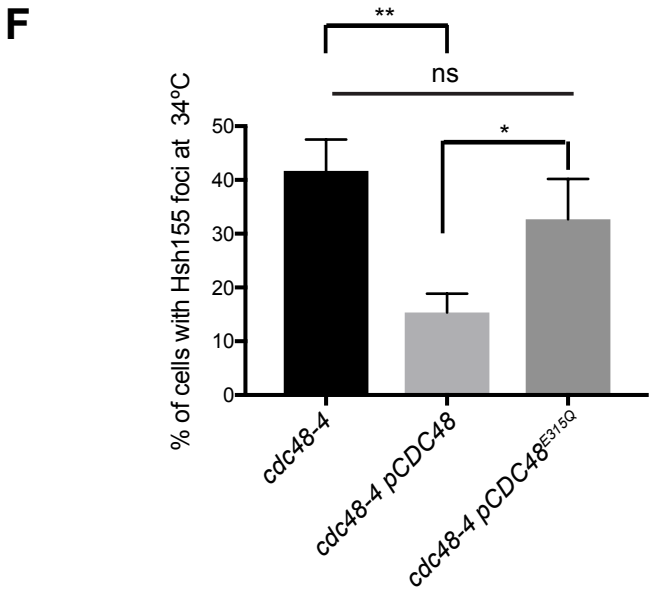

Figure3

Mathew et.al

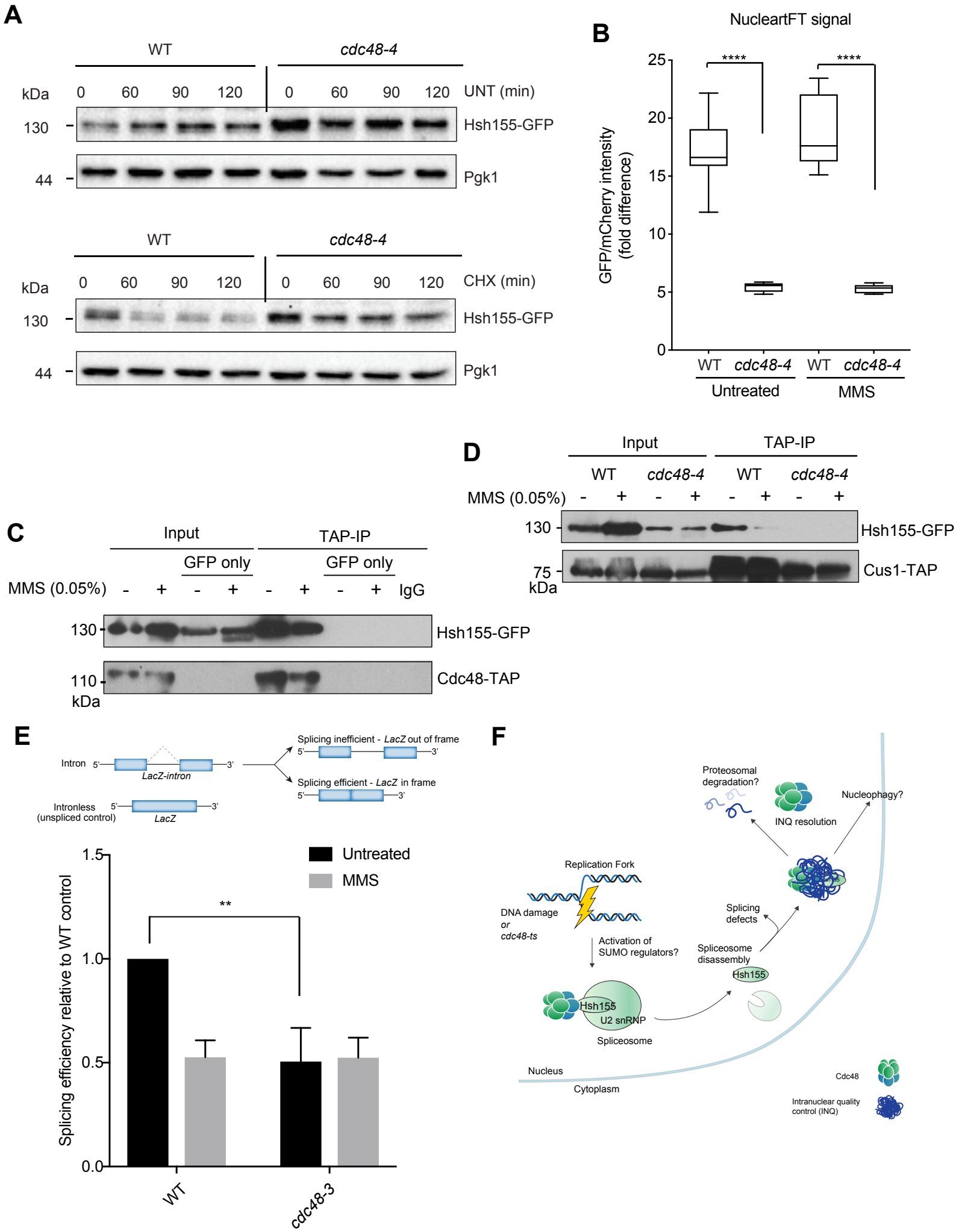

A

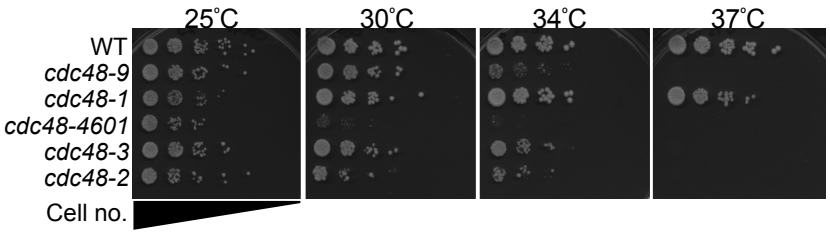

**cdc48-4601 allele referred to as cdc48-4*

B

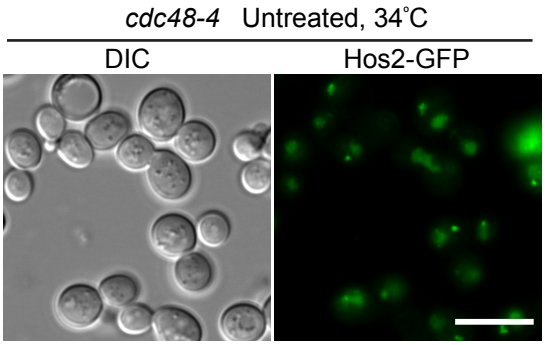

C

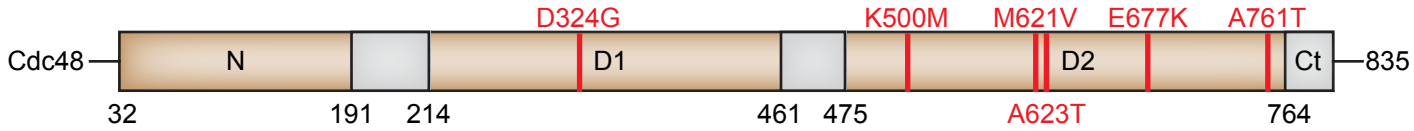

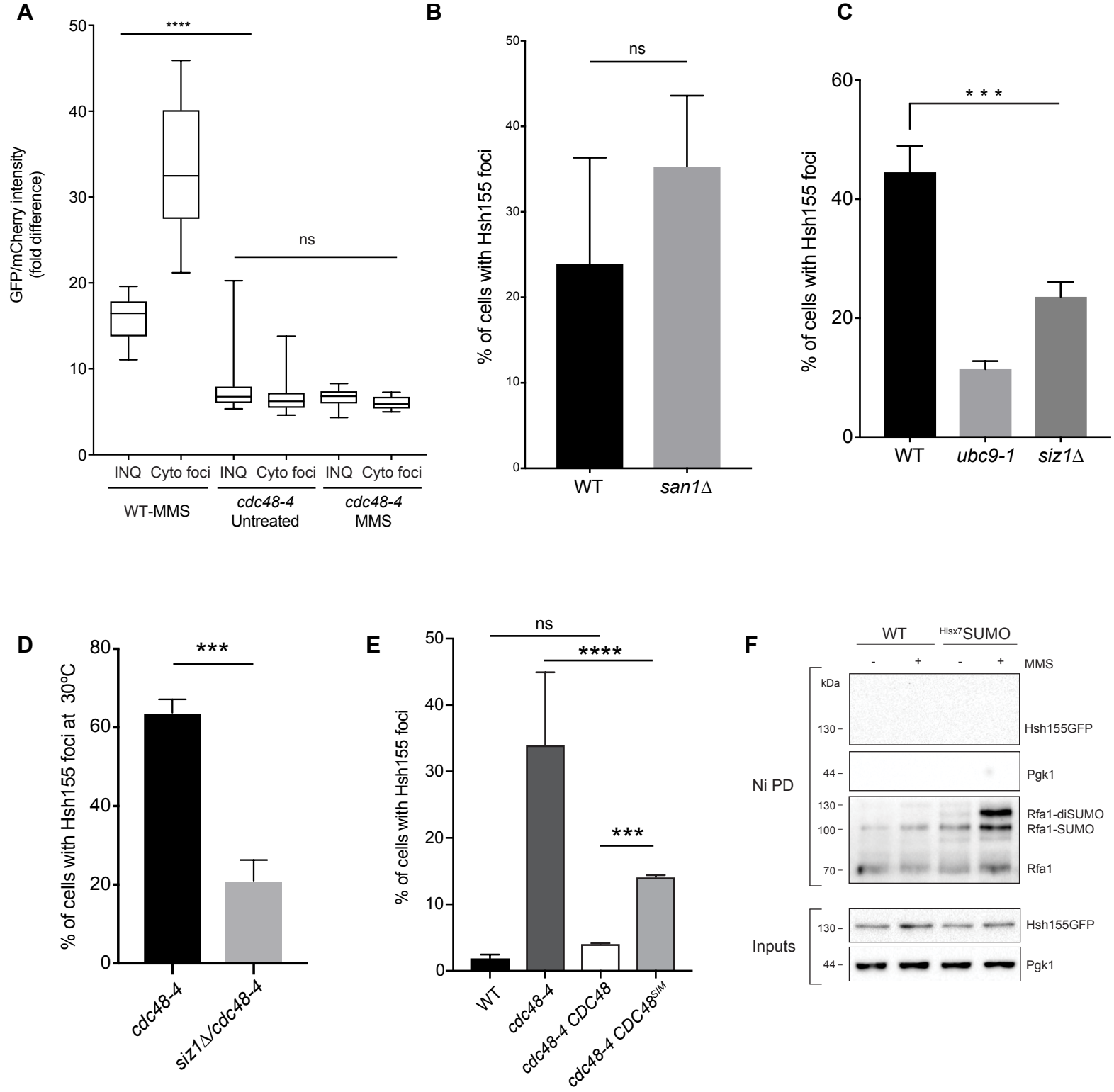
A
GFP/mCherry intensity (fold difference)
****
ns
INQ
Cyto foci
WT-MMS
cdc48-4 Untreated
cdc48-4 MMS
B
% of cells with Hsh155 foci
ns
WT
san1Δ
C
% of cells with Hsh155 foci
* * *
WT
ubc9-1
siz1Δ
D
% of cells with Hsh155 foci at 30°C
***
cdc48-4
siz1Δ/cdc48-4
E
% of cells with Hsh155 foci
ns
****
***
WT
cdc48-4
cdc48-4 CDC48
cdc48-4 CDC48SIM
F
WT
Hisx7SUMO
MMS
kDa
Hsh155GFP
Pgk1
Rfa1-diSUMO
Rfa1-SUMO
Rfa1
Ni PD
Inputs

Table S1. **Yeast strains, primers, and plasmids used in this study**

Yeast Strains (*All strains are derivatives of s288c)

Strain description	Reference number	Relevant genotype
BY4741	PSY153	MATa *ura3Δ0 leu2Δ0 his3Δ1 met15Δ0*
Cdc48-GFP	PSY1449	MATa *ura3Δ0 leu2Δ0 met15Δ0 or MET15 CDC48-GFP::HIS3*
Hsh155-GFP	PSY1502	MATa *ura3Δ0 leu2Δ0 met15Δ0 or MET15 HSH155-GFP::HIS3*
Cdc48-GFP, Hos2-mCherry	PSYL1087	MATa *ura3Δ0 leu2Δ0 met15Δ0 or MET15 CDC48-GFP::HIS3 HOS2-mCherry::CaURA3*
hos2Δ, Cdc48-GFP	PSYL727	MATα *leu2Δ0 met15Δ0 or MET15 ura3Δ0 hos2Δ::KanMX CDC48-GFP::HIS3*
*btn2Δ,*Cdc48-GFP	PSYL725	MATα *leu2Δ0 met15Δ0 or MET15 ura3Δ0 btn2Δ::KanMX CDC48-GFP::HIS3*
cdc48-4601-ts, Hsh155-GFP	PSYL721	MATa *leu2Δ0 met15Δ0 or MET15 ura3Δ0 cdc48-4601ts::KanMX HSH155-GFP::HIS3*
cdc48-2-ts, Hsh155-GFP	PSYL991	MATa *leu2Δ0 met15Δ0 or MET15 ura3Δ0 cdc48-2ts::KanMX HSH155-GFP::HIS3*
cdc48-3-ts, Hsh155-GFP	PSYL996	MATa *leu2Δ0 met15Δ0 or MET15 ura3Δ0 cdc48-3ts::KanMX HSH155-GFP::HIS3*
Hsh155-mCherry-sfGFP	PSYL733	MATa *ura3Δ0 leu2Δ0 his3Δ1 met15Δ0 HSH155-mCherry-sfGFP::KanMX*
cdc48-4601-ts, Hsh155-mCherry-sfGFP	PSYL1216	MATa *ura3Δ0 leu2Δ0 his3Δ1 met15Δ0 HSH155-mCherry-sfGFP::HygMX cdc48-4601ts::KanMX*
Hsh155-GFP, Cdc48-TAP	PSYL1125	MATα *leu2Δ0 met15Δ0 or MET15 ura3Δ0 CDC48-TAP::HIS3 HSH155-GFP::HIS3*
cdc48-4601-ts, Hsh155-GFP, Cus1-TAP	PSYL1002	MATa *leu2Δ0 met15Δ0 or MET15 ura3Δ0 CUS1-TAP::HIS3 HSH155-GFP::HIS3 cdc48-4601ts::KanMX*
Hsh155-GFP, Cus1-TAP	PSYL881	MATα *leu2Δ0 met15Δ0 or MET15 ura3Δ0 CUS1-TAP::HIS3 HSH155-GFP::HIS3*
cdc48-4601-ts, Hos2-GFP	PSYL723	*MATa leu2Δ0 met15Δ0 or MET15 ura3Δ0 cdc48-4601ts::KanMX HOS2-GFP::HIS3*
san1Δ, Hsh155-GFP	PSYL1097	MATα *leu2Δ0 met15Δ0 or MET15 ura3Δ0 san1Δ::KanMX HSH155-GFP::HIS3*
ubc9-1-ts, Hsh155-GFP	PSYL873	MATα *leu2Δ0 met15Δ0 or MET15 ura3Δ0 ubc9-1::KanMX HSH155-GFP::HIS3*
siz1Δ, Hsh155-GFP	PSYL1218	MATa *leu2Δ0 met15Δ0 or MET15 ura3Δ0 siz1Δ::KanMX HSH155-GFP::HIS3*
cdc48-4601-ts, siz1Δ, Hsh155-GFP	PSYL1301	MATa *leu2Δ0 met15Δ0 or MET15 ura3Δ0 cdc48-4601ts::KanMX siz1Δ::KanMX HSH155-GFP::HIS3*
cdc48-4601-ts, pCDC48, Hsh155-GFP	PSYL1380	MATα *leu2-112-URA3-leu2-k; cdc48-4601ts::KanMX; pYC: TRP1 CDC48 HSH155-GFP::HIS3*
cdc48-4601-ts, pcdc48SIMmut , Hsh155-GFP	PSYL1382	MATα *leu2-112-URA3-leu2-k; cdc48-4601ts::KanMX; pYC: TRP1 cdc48SIMmut HSH155-GFP::HIS3*

Primers used in this study		
Primer name		**Primer sequence (5'-3')**
Hsh155-tFT-F		CCCCGTTACACCAGACAACAATGAAGAATATATAGAAGAACTGGATTTAGTTCTGCGTACGCTGCAGGTCGAC
Hsh155-tFT-R		GTCAAGTAAAATATTCTTACAAGTTGTGGTTATTTATATGCTCTATATATATTCAATCGATGAATTCGAGCTCG
Cdc48-1-600-F		CTGGGAAGGTGAGCCAATCAACAGG
Cdc48-600-1200-F		CTGATGATGTTGATTTGGAAGCATTGG
Cdc48-1200-1800-F		CGGATAGAGTCGTCAACCAACTATTAAC
Plasmids used in this study		
Plasmid description		**Relevant Features**
pMaM17		*AmpR mCherry-sfGFP-KanMX*
pJCR51- intron version of LacZ gene (for splicing efficiency)		*AmpR CEN pJCR51::LEU2*
pLGSD5- intronless version of LacZ gene (used for normalization)		*AmpR CEN pLGSD5::LEU2*
pRG3094		*AmpR CEN pRG3094-cdc48-myc::URA3*
pRG4061		*AmpR CEN pRG3094-cdc48 E315Q-myc::URA3*